Mixed and multipoint finite element methods for rotation-based poroelasticity

Boon, W. M.; Fumagalli, A.; Scotti, A.

MIXED AND MULTIPOINT FINITE ELEMENT METHODS FOR ROTATION-BASED POROELASTICITY[*]

WIETSE M. BOON[†], ALESSIO FUMAGALLI[†], AND ANNA SCOTTI[†]

Abstract. This work proposes a mixed finite element method for the Biot poroelasticity equations that employs the lowest-order Raviart-Thomas finite element space for the solid displacement and piecewise constants for the fluid pressure. The method is based on the formulation of linearized elasticity as a weighted vector Laplace problem. By introducing the solid rotation and fluid flux as auxiliary variables, we form a four-field formulation of the Biot system, which is discretized using conforming mixed finite element spaces. The auxiliary variables are subsequently removed from the system in a local hybridization technique to obtain a multipoint rotation-flux mixed finite element method. Stability and convergence of the four-field and multipoint mixed finite element methods are shown in terms of weighted norms, which additionally leads to parameter-robust preconditioners. Numerical experiments confirm the theoretical results.

Key words. Biot poroelasticity, multipoint mixed finite element methods, weighted norms

AMS subject classifications. 65N12, 65N22, 65N30

1. Introduction. The cornerstone of this work is a reformulation of the linearized elasticity equations as a weighted vector-Laplacian on the displacement. The key is then to consider the mixed formulation of this problem by introducing the solid rotation as an auxiliary variable. This allows us to relieve the H^1-regularity requirement that is typically placed on the displacement variable.

Rotation-based formulations of elasticity and poroelasticity were recently investigated in [8] and [7], where the displacement is sought in H^1 and the rotation in L^2. In contrast, we seek the displacement in the larger space $H(\nabla\cdot, \Omega)$ and the rotation in the smaller space $H(\nabla\times, \Omega)$. In turn, our variational problem requires its own, distinct *a priori* analysis and leads to a different choice of the finite element spaces.

An important advantage of the four-field formulation we consider is that it allows for mass-lumping techniques that are common to multipoint mixed finite element methods. The primary example of these methods is the *multipoint flux mixed finite element method (MF-MFEM)* [20]. The method, traditionally employed for elliptic problems such as Darcy's flow, employs the Brezzi-Douglas-Marini [11] space to model the Darcy flux and introduces a low-order quadrature rule on its inner product to obtain an approximation of the mass matrix that is easily invertible. In turn, the flux variable can be eliminated locally, leading to a scheme with cell-centered pressures that is closely related to the multipoint flux approximation (MPFA) finite volume method [2].

The MF-MFEM was extended to the case of linearized elasticity as the *multipoint stress MFEM (MS-MFEM)* [4], which has in turn been applied to the Biot equations [5] and Stokes flow [12]. From the perspective of exterior calculus, these hybridization techniques were recognized as a way to compute local coderivatives and subsequently generalized to a larger class of mixed finite element spaces [14]. Based on these results, the *multipoint vorticity MFEM (MV-MFEM)* was recently developed for a

vorticity-velocity-pressure formulation of Stokes [10].

The similarities between the Stokes and the Biot equations were used in [19] to construct stabilized mixed finite element discretizations. Through a similar observation, we herein extend MV-MFEM for Stokes [10] to a *multipoint rotation mixed finite element method (MR-MFEM)* for linearized elasticity and poroelasticity. As mentioned before, we obtain the MR-MFEM from a rotation-based formulation of elasticity. It therefore employs the Raviart-Thomas ($\mathbb{RT}_0$) space for the solid displacement, as opposed to piecewise constants ($\mathbb{P}_0^n$) in MS-MFEM. The coupling with fluid flow in a poroelastic setting is then naturally incorporated because the divergence of the displacement is well-defined on $\mathbb{RT}_0$.

The paper is organized as follows. First, the conventions concerning notation are introduced in Subsection 1.1 and the model problem is presented in Section 2. The ensuing sections contain the main contributions of this work, which are as follows:

- Well-posedness analysis of a rotation-based, four-field formulation of poroelasticity with the solid rotation in $H(\nabla\times, \Omega)$ and displacement in $H(\nabla\cdot, \Omega)$, using parameter-weighted norms (Section 3).
- Stability and convergence analysis of two families of mixed finite elements that conform to the four-field formulation (Section 4).
- A stable and convergent multipoint rotation-flux mixed finite element method for the Biot equations that employs the $\mathbb{RT}_0 \times \mathbb{P}_0$ pair for the solid displacement and fluid pressure (Section 5).
- Parameter-robust preconditioners for the mixed finite element methods based on the analysis in weighted norms (Section 6).
- Numerical experiments that confirm the convergence of the methods and robustness of the preconditioner (Section 7).

Concluding remarks are given in Section 8.

1.1. Preliminaries and notation. Let $\Omega \subset \mathbb{R}^n$ be a contractible, Lipschitz domain with $n \in \{2, 3\}$. Let $L^2(\Omega)$ be the space of square integrable functions on Ω and let its inner product be denoted by $\langle \cdot, \cdot \rangle_\Omega$. The space $L^2(\Omega)$ is endowed with the norm $\| \cdot \| := \sqrt{\langle \cdot, \cdot \rangle_\Omega}$. We apply the same notation for the inner product and norm of square-integrable vector functions in $(L^2(\Omega))^n$.

Let $H(\nabla\cdot, \Omega)$ be the subspace of $(L^2(\Omega))^n$ that contains functions with square integrable divergence. Let $\nabla\times$ denote the conventional curl operator in 3D. Note that for $n = 2$, we simply have that $\nabla \times r := (-\partial_2 r, \partial_1 r)$ and $\nabla \times u := \partial_2 u_1 - \partial_1 u_2$ for sufficiently regular scalar fields r and vector fields u. In turn, let $H(\nabla\times, \Omega)$ be the subspace of $(L^2(\Omega))^{k_n}$, with $k_n := \binom{n}{2}$, consisting of functions with square integrable curl.

For a Hilbert space X, let X' denote its dual, and the corresponding duality pairing is given by $\langle \cdot, \cdot \rangle_{X' \times X}$. For notational brevity, we omit the subscript on duality pairings since it can be deduced from context. Given an operator $A : Z \to Y$ and a subspace $X \subseteq Z$, let $A|_X$ be the restriction of A on X. We denote the kernel and range of the restriction by $\text{Ker}(A, X) := \text{Ker}(A|_X)$ and $\text{Ran}(A, X) := \text{Ran}(A|_X)$, respectively.

For $a, b \in \mathbb{R}$, the notation $a \lesssim b$ implies that a constant $C > 0$ exists, independent of material or discretization parameters, such that $Ca \leq b$. However, the constant C may depend on the domain Ω and on the shape-regularity of the mesh. We use $\gtrsim$ analogously and $a \approx b$ if and only if $a \lesssim b \lesssim a$.

2. Model Problem. We start in Subsection 2.1 with linear elasticity to highlight the manipulation of the system that lies at the heart of the proposed numerical

methods. The coupling to flow is introduced afterward in Subsection 2.2.

2.1. Linearized elasticity as a weighted vector-Laplacian. Let us consider the governing equations of linearized elasticity in terms of the Cauchy stress σ and displacement u:

$$(2.1) \qquad \sigma = 2\mu\varepsilon(u) + (\lambda\nabla \cdot u)I, \qquad\qquad -\nabla \cdot \sigma = f_u.$$

Here, μ and λ are the Lamé parameters, f_u is a body force, ε is the symmetric gradient and $I \in \mathbb{R}^{n\times n}$ the identity tensor. We reformulate these equations by recalling the following calculus identity:

$$(2.2) \qquad -\nabla \cdot \varepsilon(u) = \frac{1}{2}\nabla \times (\nabla \times u) - \nabla(\nabla \cdot u).$$

We substitute this identity and the definition of σ in the momentum balance equation and assume spatially constant μ to obtain

$$(2.3) \qquad \nabla \times (\mu\nabla \times u) - \nabla(2\mu + \lambda)\nabla \cdot u = f_u$$

We now define the rotation variable $r := \mu\nabla \times u$, which leads us to the strong form of our 2-field formulation for linear elasticity in terms of (r, u):

$$(2.4a) \qquad \mu^{-1}r - \nabla \times u = 0, \qquad\qquad \nabla \times r - \nabla(2\mu + \lambda)\nabla \cdot u = f_u.$$

subject to the boundary conditions

$$(2.4b) \qquad \begin{aligned} \nu \cdot u &= 0, & \nu \times r &= 0, & \text{on } \partial_r\Omega, \\ \nu \times u &= \nu \times u_0, & (2\mu + \lambda)\operatorname{Tr}\varepsilon(u) &= \sigma_0, & \text{on } \partial_u\Omega. \end{aligned}$$

Here, $\partial_r\Omega \cup \partial_u\Omega$ is a disjoint decomposition of the boundary $\partial\Omega$ and ν is its outward oriented, unit normal vector. To ensure uniqueness, we assume that the boundary decomposition is such that $\|\nu \cdot \phi\|_{\partial_r\Omega} + \|\nu \times \phi\|_{\partial_u\Omega} > 0$ for all non-zero rigid body motions ϕ.

To derive the variational formulation of (2.4), we introduce the following Hilbert spaces in which to seek the rotation and displacement variables:

$$(2.5) \qquad \begin{aligned} R &:= \{r \in H(\nabla\times, \Omega) \mid \nu \times r = 0 \text{ on } \partial_r\Omega\}, \\ U &:= \{u \in H(\nabla\cdot, \Omega) \mid \nu \cdot u = 0 \text{ on } \partial_r\Omega\}. \end{aligned}$$

By introducing test functions $(\tilde{r}, \tilde{u}) \in R \times U$ and using integration by parts, we obtain the variational formulation: find $(\tilde{r}, \tilde{u}) \in R \times U$ such that

$$(2.6) \qquad \begin{aligned} \langle\mu^{-1}r, \tilde{r}\rangle_\Omega - \langle u, \nabla \times \tilde{r}\rangle_\Omega &= \langle u_0, \nu \times \tilde{r}\rangle_{\partial_u\Omega}, & \forall\tilde{r} \in R, \\ \langle\nabla \times r, \tilde{u}\rangle_\Omega + \langle(2\mu + \lambda)\nabla \cdot u, \nabla \cdot \tilde{u}\rangle_\Omega &= \langle f_u, \tilde{u}\rangle_\Omega - \langle\sigma_0, \nu \cdot \tilde{u}\rangle_{\partial_u\Omega}, & \forall\tilde{u} \in U. \end{aligned}$$

REMARK 2.1. *The boundary conditions in (2.4) do not immediately translate into classical boundary conditions such as clamped boundaries, i.e. $u = 0$ on $\partial\Omega$. We refer to [9] for techniques that handle this case.*

3

2.2. Coupling to porous medium flow. Next, we consider the setting of a poroelastic medium in which fluid flow and solid mechanics form a fully coupled system known as the quasi-steady Biot equations:

$$
\begin{aligned}
(2.7) \qquad &\sigma = 2\mu\varepsilon(u) + (\lambda\nabla \cdot u - \alpha p)I, &&-\nabla \cdot \sigma = f_u, \\
&\check{q} = -K\nabla p, &&\partial_t(c_0 p + \alpha\nabla \cdot u) + \nabla \cdot \check{q} = \check{f}_p,
\end{aligned}
$$

with $\check{q}$ the Darcy flux and p the fluid pressure. Moreover, K is the hydraulic conductivity, c_0 the specific storativity, and α is the Biot-Willis constant.

Using the same steps as in Subsection 2.1, we rewrite the elasticity equations in terms of rotation and displacement. As time discretization, we choose an implicit method such as the backward Euler or Crank-Nicolson scheme with time step Δt.

In order to obtain an advantageous scaling with the time step, we introduce the scaled Darcy flux $q := \delta\check{q}$, with $\delta := \sqrt{\Delta t}$. Different scalings of $\check{q}$ are possible, but may result in systems that either do not have favorable symmetries, which complicates the analysis, or contain negative powers of Δt, which can be undesirable in the case of small time steps.

By including quantities relative to the previous time step in the right-hand side f_p, we obtain the semi-discrete, four-field formulation of the Biot equations:

$$
(2.8a) \qquad
\begin{bmatrix}
\mu^{-1} & -\nabla\times & & \\
\nabla\times & -\nabla(2\mu+\lambda)\nabla\cdot & & \nabla\alpha \\
& & K^{-1} & \delta\nabla \\
& \alpha\nabla\cdot & \nabla\cdot\delta & c_0
\end{bmatrix}
\begin{bmatrix} r \\ u \\ q \\ p \end{bmatrix}
=
\begin{bmatrix} 0 \\ f_u \\ 0 \\ f_p \end{bmatrix},
$$

subject to the boundary conditions

$$
(2.8b) \qquad
\begin{aligned}
\nu \cdot u &= 0, & \nu \times r &= 0, & &\text{on } \partial_r\Omega, \\
\nu \times u &= \nu \times u_0, & (2\mu+\lambda)\operatorname{Tr}\varepsilon(u) - \alpha p &= \sigma_0, & &\text{on } \partial_u\Omega, \\
p &= p_0, \text{ on } \partial_p\Omega, & \nu \cdot q &= 0, & &\text{on } \partial_q\Omega.
\end{aligned}
$$

We assume that $\partial_p\Omega \cup \partial_q\Omega$ forms a disjoint decomposition of the boundary with $|\partial_p\Omega| > 0$. To facilitate the analysis in the next section, we define the following Hilbert spaces for the fluid flux and pressure:

$$
(2.9) \qquad Q := \{q \in H(\nabla\cdot,\Omega) \mid \nu \cdot q = 0 \text{ on } \partial_q\Omega\}, \qquad P := L^2(\Omega).
$$

3. Analysis of the semi-discrete problem. We continue by constructing and analyzing the variational formulation of system (2.8), which is continuous in space and discrete in time. As short-hand notation, we will use $x := (r, u, q, p)$ and $\tilde{x} := (\tilde{r}, \tilde{u}, \tilde{q}, \tilde{p})$ belonging to the Hilbert space:

$$
(3.1) \qquad X := R \times U \times Q \times P,
$$

with the spaces R, U defined in (2.5) and Q, P in (2.9).

For simplicity, let all material parameters be homogenous in space and we moreover assume that the conductivity K is isotropic and thus given by a positive scalar. To highlight the structure of the system, we define the operators $A : X \to X'$ and $B : X \to X'$ and the functional $f \in X'$ as follows:

$$
\begin{aligned}
\langle Ax, \tilde{x}\rangle &:= \mu^{-1}\langle r, \tilde{r}\rangle_\Omega + (2\mu+\lambda)\langle\nabla \cdot u, \nabla \cdot \tilde{u}\rangle_\Omega + K^{-1}\langle q, \tilde{q}\rangle_\Omega + c_0\langle p, \tilde{p}\rangle_\Omega, \\
\langle Bx, \tilde{x}\rangle &:= \langle\nabla \times r, \tilde{u}\rangle_\Omega + \langle\nabla \cdot (\alpha u + \delta q), \tilde{p}\rangle_\Omega, \\
\langle f, \tilde{x}\rangle &:= \langle u_0, \nu \times \tilde{r}\rangle_{\partial_u\Omega} + \langle f_u, \tilde{u}\rangle_\Omega - \langle\sigma_0, \nu \cdot \tilde{u}\rangle_{\partial_u\Omega} - \langle p_0, \nu \cdot \delta\tilde{q}\rangle_{\partial_p\Omega} + \langle f_p, \tilde{p}\rangle_\Omega.
\end{aligned}
$$

4

Let the compound operator $\mathcal{A} : X \to X'$ be such that

$$(3.2) \qquad \mathcal{A} := A + B - B^*,$$

with $B^* : X \to X'$ the adjoint of B defined by $\langle B^* x, \tilde{x} \rangle := \langle B\tilde{x}, x \rangle$.

The variational formulation of (2.8) is then given by: find $x \in X$ such that

$$(3.3) \qquad \langle \mathcal{A}x, \tilde{x} \rangle = \langle f, \tilde{x} \rangle, \qquad\qquad \forall \tilde{x} \in X.$$

Based on the scaling in the operator $\mathcal{A}$, we endow X with the following parameter-dependent norm:

$$\|x\|_X^2 := \mu^{-1}(\|r\|^2 + \|\nabla \times r\|^2) + \mu\|u\|^2 + (2\mu + \lambda)\|\nabla \cdot u\|^2$$
$$(3.4) \qquad + K^{-1}\|q\|^2 + \frac{\delta^2}{\eta + c_0}\|\nabla \cdot q\|^2 + (\eta + c_0)\|p\|^2.$$

3Here, $\eta := \frac{\alpha^2}{2\mu + \lambda} + \delta^2 K$ is a scaling parameter particularly chosen for the ensuing analysis. In order for these norms to be well-defined, we assume that μ, λ, K, and $(\eta + c_0)$ are positive. However, we do not explicitly bound these parameters away from zero, so that we do not rely on small, lower bounds in our analysis.

It is convenient to analyze problem (3.3) using an equivalent energy norm, which we introduce in the following lemma.

LEMMA 3.1 (Energy norm). *Let Π be the L^2-projection onto $\mathrm{Ran}(\nabla \times, R)$ and let the energy norm be given by*

$$\||x\||^2 := \mu^{-1}(\|r\|^2 + \|\nabla \times r\|^2) + \mu\|\Pi u\|^2 + (2\mu + \lambda)\|\nabla \cdot u\|^2$$
$$(3.5) \qquad + K^{-1}\|q\|^2 + \frac{1}{\eta + c_0}\|\nabla \cdot (\alpha u + \delta q)\|^2 + (\eta + c_0)\|p\|^2.$$

Then the following equivalence holds:

$$(3.6) \qquad \|x\|_X \eqsim \||x\||, \qquad\qquad \forall x \in X.$$

Proof. Let us consider the lower bound "$\gtrsim$". We first show that $\|u\| \gtrsim \|\Pi u\|$ follows immediately from the L^2-orthogonality of Π:

$$(3.7a) \qquad \|u\|^2 = \|\Pi u\|^2 + \|(I - \Pi)u\|^2 \geq \|\Pi u\|^2.$$

Secondly, we consider the norms on the divergence terms. The triangle-type inequality $\|a + b\|^2 \leq 2(\|a\|^2 + \|b\|^2)$ and the lower bound $\eta + c_0 \geq \frac{\alpha^2}{2\mu + \lambda}$ yield

$$\frac{1}{\eta + c_0}\|\nabla \cdot (\alpha u + \delta q)\|^2 \leq 2\left(\frac{\alpha^2}{\eta + c_0}\|\nabla \cdot u\|^2 + \frac{\delta^2}{\eta + c_0}\|\nabla \cdot q\|^2\right)$$
$$(3.7b) \qquad\qquad \leq 2\left((2\mu + \lambda)\|\nabla \cdot u\|^2 + \frac{\delta^2}{\eta + c_0}\|\nabla \cdot q\|^2\right).$$

Collecting (3.7), we conclude $\|x\|_X \gtrsim \||x\||$.

For the upper bound "$\lesssim$", we once again first bound the norm $\|u\|$. The Poincaré inequality implies that a $\alpha_u > 0$ exists such that

$$\alpha_u\|u\| \leq \|\nabla \cdot u\|, \qquad\qquad \forall u \perp \mathrm{Ker}(\nabla \cdot, U).$$

5

Since Ω is contractible, we have $\mathrm{Ker}(\nabla\cdot, U) = \mathrm{Ran}(\nabla\times, R)$ and we use the Poincaré inequality to derive

$$\mu\|u\|^2 \leq \mu\|\Pi u\|^2 + \frac{1}{\alpha_u^2}\mu\|\nabla\cdot((I-\Pi)u)\|^2$$

$$= \mu\|\Pi u\|^2 + \frac{1}{\alpha_u^2}\mu\|\nabla\cdot u\|^2$$

$$(3.8a) \qquad \leq \max\left\{\frac{1}{2\alpha_u^2}, 1\right\}\left(\mu\|\Pi u\|^2 + (2\mu+\lambda)\|\nabla\cdot u\|^2\right).$$

It remains to show a bound on the divergence terms. Using the same triangle-type inequality and lower bound on $\eta + c_0$ as in (3.7b), we derive

$$\frac{1}{\eta+c_0}\|\nabla\cdot(\alpha u + \delta q)\|^2 \geq \frac{1}{\eta+c_0}\left(\frac{1}{2}\|\nabla\cdot\delta q\|^2 - \|\nabla\cdot\alpha u\|^2\right)$$

$$\geq \frac{1}{2}\frac{\delta^2}{\eta+c_0}\|\nabla\cdot q\|^2 - (2\mu+\lambda)\|\nabla\cdot u\|^2.$$

From this result, we deduce

$$(2\mu+\lambda)\|\nabla\cdot u\|^2 + \frac{1}{\eta+c_0}\|\nabla\cdot(\alpha u + \delta q)\|^2$$

$$\geq (2\mu+\lambda)\|\nabla\cdot u\|^2 + \frac{2}{3}\frac{1}{\eta+c_0}\|\nabla\cdot(\alpha u + \delta q)\|^2$$

$$(3.8b) \qquad \geq \frac{1}{3}\left((2\mu+\lambda)\|\nabla\cdot u\|^2 + \frac{\delta^2}{\eta+c_0}\|\nabla\cdot q\|^2\right).$$

Collecting (3.8), we have $\|x\|_X \lesssim \|\|x\|\|$ and the result follows. $\qquad\square$

With the energy norm defined by (3.5), we are now ready to prove the key prerequisites for well-posedness of (3.3), namely the continuity and inf-sup conditions on $\mathcal{A}$.

LEMMA 3.2 (Continuity). *The operator $\mathcal{A}: X \to X'$ is continuous:*

$$(3.9) \qquad \|\mathcal{A}x\| := \sup_{\tilde{x}\in X}\frac{\langle\mathcal{A}x, \tilde{x}\rangle}{\|\tilde{x}\|_X} \lesssim \|x\|_X, \qquad\qquad \forall x \in X.$$

Proof. First, we apply the Cauchy-Schwarz inequality to each of the terms, e.g.

$$\mu^{-1}\langle r, \tilde{r}\rangle_\Omega \leq \mu^{-1}\|r\|\|\tilde{r}\|, \qquad \langle\nabla\times r, \tilde{u}\rangle_\Omega = \langle\nabla\times r, \Pi\tilde{u}\rangle_\Omega \leq \frac{1}{\sqrt{\mu}}\|r\|\sqrt{\mu}\|\Pi\tilde{u}\|.$$

After summing all products, we use the Cauchy-Schwarz once more to conclude that $\langle\mathcal{A}x, \tilde{x}\rangle \lesssim \|\|x\|\| \, \|\|\tilde{x}\|\|$. The result in $\|\cdot\|_X$ follows from the norm equivalence shown in Lemma 3.1. $\qquad\square$

LEMMA 3.3 (Inf-sup). *The operator $\mathcal{A}$ is bounded from below as*

$$(3.10) \qquad \|\mathcal{A}x\| \gtrsim \|x\|_X, \qquad\qquad \forall x \in X.$$

Proof. We aim to show that, for given $x \in X$, a test function $\tilde{x} \in X$ exists with the properties

$$(3.11) \qquad \langle\mathcal{A}x, \tilde{x}\rangle \gtrsim \|\|x\|\|^2, \qquad\qquad \|\|\tilde{x}\|\| \lesssim \|\|x\|\|.$$

The equivalence from Lemma 3.1 will then provide the result in the norm $\|\cdot\|_X$.

We construct this test function explicitly in four parts. First, let $\tilde{x}_0 := x = (r, u, q, p)$ for which we derive

(3.12) $\qquad \langle \mathcal{A}x, \tilde{x}_0 \rangle = \langle Ax, x \rangle = \mu^{-1}\|r\|^2 + (2\mu + \lambda)\|\nabla \cdot u\|^2 + K^{-1}\|q\|^2 + c_0\|p\|^2.$

The second test function we consider is given by $\tilde{x}_1 := (0, \mu^{-1}\nabla \times r, 0, \frac{1}{\eta_0 + c_0}\nabla \cdot (\alpha u + \delta q))$ with $\eta_0 \geq 0$ to be chosen later. Using the orthogonality $\nabla \cdot \nabla \times r = 0$, we derive using the Cauchy-Schwarz and Young's inequality:

$$\langle \mathcal{A}x, \tilde{x}_1 \rangle = \mu^{-1}\|\nabla \times r\|^2 + \frac{1}{\eta_0 + c_0}\|\nabla \cdot (\alpha u + \delta q)\|^2 + \langle \frac{c_0}{\eta_0 + c_0}p, \nabla \cdot (\alpha u + \delta q)\rangle_\Omega$$

$$\geq \mu^{-1}\|\nabla \times r\|^2 + \frac{1}{\eta_0 + c_0}\|\nabla \cdot (\alpha u + \delta q)\|^2 - \|p\|\|\nabla \cdot (\alpha u + \delta q)\|$$

(3.13) $\qquad \geq \mu^{-1}\|\nabla \times r\|^2 + \frac{1}{2(\eta_0 + c_0)}\|\nabla \cdot (\alpha u + \delta q)\|^2 - \frac{\eta_0 + c_0}{2}\|p\|^2.$

The last two components are constructed by exploiting the inf-sup conditions on the operators that compose B. The first of these implies that a $\beta_r > 0$ exists such that for each $u \in U$, there exists a $\tilde{r}_u \in R$ with

$$\nabla \times \tilde{r}_u = \Pi u, \qquad\qquad \beta_r \left(\|\tilde{r}_u\|^2 + \|\nabla \times \tilde{r}_u\|^2\right) \leq \|\Pi u\|^2.$$

We use $\tilde{r}_u$ to define $\tilde{x}_2 := (-\beta_r\mu\tilde{r}_u, 0, 0, 0)$. The Cauchy-Schwarz and Young inequalities give us:

$$\langle \mathcal{A}x, \tilde{x}_2 \rangle = \beta_r\mu\|\Pi u\|^2 - \beta_r\langle r, \tilde{r}_u\rangle_\Omega$$

$$\geq \beta_r\mu\|\Pi u\|^2 - \frac{1}{2}\left(\mu^{-1}\|r\|^2 + \beta_r^2\mu\|\tilde{r}_u\|^2\right)$$

(3.14) $\qquad \geq \frac{\beta_r}{2}\mu\|\Pi u\|^2 - \frac{1}{2}\mu^{-1}\|r\|^2$

The final test function is constructed similarly. Two constants $\beta_u, \beta_q > 0$ exist such that for each $p \in P$, there exists a pair $(\tilde{u}_p, \tilde{q}_p) \in U \times Q$ with the properties

$$\nabla \cdot \tilde{u}_p = p, \qquad \Pi\tilde{u}_p = 0, \qquad \beta_u \left(\|\tilde{u}_p\|^2 + \|\nabla \cdot \tilde{u}_p\|^2\right) \leq \|p\|^2,$$
$$\nabla \cdot \tilde{q}_p = p, \qquad \Pi\tilde{q}_p = 0, \qquad \beta_q \left(\|\tilde{q}_p\|^2 + \|\nabla \cdot \tilde{q}_p\|^2\right) \leq \|p\|^2$$

These allow us to define $\tilde{x}_3 := (0, -\frac{\alpha}{2\mu + \lambda}\tilde{u}_p, -\beta_q\delta K\tilde{q}_p, 0)$. Let us use the short-hand notation $\eta_0 := \frac{1}{2}\left(\frac{\alpha^2}{2\mu + \lambda} + \beta_q\delta^2 K\right)$. We then proceed as in (3.14) to derive

$$\langle \mathcal{A}x, \tilde{x}_3 \rangle = \left(\frac{\alpha^2}{2\mu + \lambda} + \beta_q\delta^2 K\right)\|p\|^2 - \alpha\langle \nabla \cdot u, p\rangle_\Omega - \beta_q\delta\langle q, \tilde{q}_p\rangle_\Omega$$

$$\geq 2\eta_0\|p\|^2$$

$$- \frac{1}{2}\left((2\mu + \lambda)\|\nabla \cdot u\|^2 + \frac{\alpha^2}{2\mu + \lambda}\|p\|^2 + K^{-1}\|q\|^2 + \beta_q^2\delta^2 K\|\tilde{q}_p\|^2\right)$$

(3.15) $\qquad \geq \eta_0\|p\|^2 - \frac{1}{2}(2\mu + \lambda)\|\nabla \cdot u\|^2 - \frac{1}{2}K^{-1}\|q\|^2.$

Letting $\tilde{x} := \sum_i \tilde{x}_i$, we sum (3.12), (3.13), (3.14), and (3.15) to obtain

$$\langle \mathcal{A}x, \tilde{x} \rangle \geq \frac{1}{2} \left(\mu^{-1}\|r\|^2 + \frac{2}{\mu}\|\nabla \times r\|^2 + \beta_r \mu \|\Pi u\|^2 + (2\mu + \lambda)\|\nabla \cdot u\|^2 \right.$$

$$\left. + \frac{1}{\eta_0 + c_0}\|\nabla \cdot (\alpha u + \delta q)\|^2 + K^{-1}\|q\|^2 + (\eta_0 + c_0)\|p\|^2 \right)$$

$$(3.16) \qquad \gtrsim \|\|x\|\|^2,$$

where we used $\eta_0 \eqsim \eta$ in the final inequality since $\min\{1, \beta_q\}\eta \leq 2\eta_0 \leq \max\{1, \beta_q\}\eta$.

It remains to show that $\tilde{x}$ is bounded. Clearly, we have $\|\|\tilde{x}_0\|\| = \|\|x\|\|$, so we continue with the bounds for the remaining x_i:

$$\|\|\tilde{x}_1\|\|^2 = \mu\|\mu^{-1}\nabla \times r\|^2 + \frac{\eta + c_0}{(\eta_0 + c_0)^2}\|\nabla \cdot (\alpha u + \delta q)\|^2$$

$$\lesssim \mu^{-1}\|\nabla \times r\|^2 + \frac{1}{\eta + c_0}\|\nabla \cdot (\alpha u + \delta q)\|^2 \leq \|\|x\|\|^2$$

$$(3.17) \qquad \|\|\tilde{x}_2\|\|^2 = \mu\beta_r^2(\|\tilde{r}_u\|^2 + \|\nabla \times \tilde{r}_u\|^2) \lesssim \mu\|\Pi u\|^2 \leq \|\|x\|\|^2$$

$$\|\|\tilde{x}_3\|\|^2 = \frac{\alpha^2}{2\mu + \lambda}\|p\|^2 + \beta_q^2 \delta^2 K\|\tilde{q}_p\|^2 + \frac{1}{\eta + c_0}\|2\eta_0 p\|^2$$

$$\lesssim \eta\|p\|^2 \leq \|\|x\|\|^2.$$

Collecting (3.17), we have $\|\|\tilde{x}\|\| \lesssim \|\|x\|\|$. Together with (3.16), we have shown (3.11) and the result follows by Lemma 3.1. $\square$

THEOREM 3.4 (Well-posedness). *Problem* (3.3) *admits a unique solution $x \in X$ that satisfies*

$$(3.18) \qquad \|x\|_X \lesssim \|f\|_{X'} := \sup_{\tilde{x} \in X} \frac{\langle f, \tilde{x} \rangle}{\|\tilde{x}\|_X}.$$

Proof. We aim to utilize the Babuška-Lax-Milgram theorem. For this, we need to show that for each $x \in X$, a $\tilde{x} \in X$ exists such that $\langle \mathcal{A}\tilde{x}, x \rangle > 0$. The symmetries of $\mathcal{A}$ allow us to write:

$$(3.19) \qquad \langle \mathcal{A}\tilde{x}, x \rangle = \langle \mathcal{A}(\tilde{r}, \tilde{u}, \tilde{q}, \tilde{p}), (r, u, q, p) \rangle = \langle \mathcal{A}(r, -u, -q, p), (\tilde{r}, -\tilde{u}, -\tilde{q}, \tilde{p}) \rangle$$

In turn, we use Lemma 3.3 to construct $\tilde{x}$ such that $\langle \mathcal{A}\tilde{x}, x \rangle \gtrsim \|x\|_X > 0$.

Combining (3.19) with Lemmas 3.2 and 3.3, we invoke the Babuška-Lax-Milgram theorem to conclude that a unique solution exists that satisfies (3.18) $\square$

COROLLARY 3.5. *The elasticity problem* (2.6) *admits a unique solution $(r, u) \in R \times U$ that is bounded in the norm*

$$(3.20) \qquad \|(r, u)\|_{R \times U}^2 := \mu^{-1}(\|r\|^2 + \|\nabla \times r\|^2) + \mu\|u\|^2 + (2\mu + \lambda)\|\nabla \cdot u\|^2.$$

Proof. Let $\alpha = 0$, then the system (3.3) decouples into the elasticity problem (2.6) and a Darcy flow problem. If we neglect the Darcy problem, then Theorem 3.4 gives us that the unique solution x is bounded in the norm $\|x\|_X = \|(r, u, 0, 0)\|_X = \|(r, u)\|_{R \times U}$. $\square$

4. Conforming four-field MFE discretization. In this section, we introduce a conforming mixed finite element discretization of the four-field formulation (3.3). Let Ω_h be a shape-regular, simplicial tesselation of the domain Ω. We define the discrete space $X_h := R_h \times U_h \times Q_h \times P_h$ such that the following assumptions hold

A1. The finite element spaces are conforming, i.e. $X_h \subset X$.

A2. The pairs $Q_h \times P_h$ and $U_h \times P_h$ satisfy

$$\mathrm{Ran}(\nabla \cdot, Q_h) = \mathrm{Ran}(\nabla \cdot, U_h) = P_h$$

and are inf-sup stable for the mixed formulation of the Poisson equation, i.e.

$$\sup_{\tilde{q}_h \in Q_h} \frac{\langle \nabla \cdot \tilde{q}_h, p_h \rangle_\Omega}{\|\tilde{q}_h\| + \|\nabla \cdot \tilde{q}_h\|} \gtrsim \|p_h\|, \quad \sup_{\tilde{u}_h \in U_h} \frac{\langle \nabla \cdot \tilde{u}_h, p_h \rangle_\Omega}{\|\tilde{u}_h\| + \|\nabla \cdot \tilde{u}_h\|} \gtrsim \|p_h\|, \quad \forall p_h \in P_h.$$

A3. The pair $R_h \times U_h$ satisfies $\mathrm{Ran}(\nabla \times, R_h) = \mathrm{Ker}(\nabla \cdot, U_h)$ and

$$\sup_{\tilde{r}_h \in R_h} \frac{\langle \nabla \times \tilde{r}_h, u_h \rangle_\Omega}{\|\tilde{r}_h\| + \|\nabla \times \tilde{r}_h\|} \gtrsim \|u_h\|, \qquad \forall u_h \in U_h.$$

REMARK 4.1. *Assumptions A2 and A3 can be relaxed to general inf-sup stable pairs of finite elements that do not satisfy* $\mathrm{Ran}(\nabla \cdot, Q_h) \subseteq P_h$, $\mathrm{Ran}(\nabla \cdot, U_h) \subseteq P_h$, *and* $\mathrm{Ran}(\nabla \times, R_h) \subseteq U_h$. *However, in order to ease the upcoming analysis, we consider these stronger assumptions.*

REMARK 4.2. *These assumptions are different from the Stokes-Biot stability conditions introduced in [19, Def. 3.1] since we do note require a Stokes-stable pair* $U_h \times P_h$. *On the other hand, we need the additional space* R_h *to capture the solid rotations.*

We focus on two families of discretizations that satisfy these assumptions. For given polynomial degree $k \geq 0$, the first of these families is given by

$$(4.1) \qquad X_h^{(1)} := \left(\mathbb{N}_k^{(1)} \times \mathbb{RT}_k \times \mathbb{RT}_k \times \mathbb{P}_k \right) \cap X.$$

In particular, the rotation variable is discretized using Nédélec elements of the first kind [17]. Here, k denotes the polynomial degree of the tangential traces on mesh edges. The displacement and fluid flux are both discretized using Raviart-Thomas elements of order k, which implies that the normal traces of these functions on mesh faces are of polynomial degree k. Finally, the pressure variable is sought in the space of discontinuous, elementwise polynomials of degree k. The intersection with X ensures that the essential boundary conditions are respected.

The second family we consider is defined as:

$$(4.2) \qquad X_h^{(2)} := \left(\mathbb{N}_{k+1}^{(2)} \times \mathbb{RT}_k \times \mathbb{BDM}_{k+1} \times \mathbb{P}_k \right) \cap X.$$

In this case, the Nédélec elements of the second kind are used to discretize the rotation variable. The notation $\mathbb{N}_{k+1}^{(2)}$ implies that the basis functions of R_h are given by polynomials of degree $k+1$ on the mesh edges. Similarly, the fluid flux is here given by the Brezzi-Douglas-Marini space $\mathbb{BDM}_{k+1}$ which has normal traces on mesh faces of polynomial degree $k+1$.

In 2D, since rotation is a scalar, the two families of discrete spaces employ the continuous Lagrange elements of order $k+1$ for the rotation space R_h, denoted by $\mathbb{L}_{k+1}$.

With the discrete space $X_h \subset X$ defined, we are ready to formulate the *four-field mixed finite element method (4F-MFEM)*: find $x_h \in X_h$ such that

$$(4.3) \qquad \langle \mathcal{A}x_h, \tilde{x}_h \rangle = \langle f, \tilde{x}_h \rangle, \qquad\qquad \forall \tilde{x}_h \in X_h.$$

The two main results are presented next, namely the stability of the 4F-MFEM in Subsection 4.1 and its convergence in Subsection 4.2.

4.1. Stability. The analysis of (4.3) follows the same steps as in Section 3. First, the continuity bound $\langle Ax_h, \tilde{x}_h \rangle \lesssim \|x_h\|_X \|\tilde{x}_h\|_X$, $\forall x_h, \tilde{x}_h \in X_h$ is immediate by Lemma 3.2 and the conformity A1. The inf-sup condition is considered in the following lemma.

LEMMA 4.1 (Inf-sup). *If X_h satisfies A1–A3, then the following bound holds*

$$(4.4) \qquad \sup_{\tilde{x}_h \in X_h} \frac{\langle \mathcal{A}x_h, \tilde{x}_h \rangle}{\|\tilde{x}_h\|_X} \gtrsim \|x_h\|_X, \qquad\qquad \forall x_h \in X_h.$$

Proof. First, we define the discrete analogue of the energy norm (3.5) as

$$|||x_h|||_h^2 := \mu^{-1}(\|r_h\|^2 + \|\nabla \times r_h\|^2) + \mu\|\Pi_h u_h\|^2 + (2\mu + \lambda)\|\nabla \cdot u_h\|^2$$
$$(4.5) \qquad\qquad + K^{-1}\|q_h\|^2 + \frac{1}{\eta + c_0}\|\nabla \cdot (\alpha u_h + \delta q_h)\|^2 + (\eta + c_0)\|p_h\|^2.$$

with Π_h the L^2-projection on $\mathrm{Ran}(\nabla \times, R_h)$. The equivalence $\|x_h\|_X \eqsim |||x_h|||_h$ holds for all $x_h \in X_h$ by the same arguments as in Lemma 3.1, using A1 and $\mathrm{Ker}(\nabla \cdot, U_h) = \mathrm{Ran}(\nabla \times, R_h)$ from assumption A3.

Next, we follow the proof of Lemma 3.3 for a discrete function $x_h \in X_h$ and Π replaced by Π_h. Each of the test functions $\tilde{x}_{h,i} \in X_h$ can be created in analogy to $\tilde{x}_i$ due to assumptions A2 and A3. Thus, defining $\tilde{x}_h := \sum_i \tilde{x}_{h,i}$, we have $\langle \mathcal{A}x_h, \tilde{x}_h \rangle \gtrsim |||x_h|||_h^2$ and $|||\tilde{x}_h|||_h \lesssim |||x_h|||_h$. The equivalence of norms then provides the result. $\square$

The stability of the mixed finite element method, which forms the main result of this section, now follows by the same arguments as in Theorem 3.4.

THEOREM 4.2 (Stability). *If assumptions A1–A3 are satisfied, then the discrete problem (4.3) admits a unique solution $x_h \in X_h$ that satisfies*

$$(4.6) \qquad \|x_h\|_X \lesssim \|f\|_{X_h'} := \sup_{\tilde{x}_h \in X_h} \frac{\langle f, \tilde{x}_h \rangle}{\|\tilde{x}_h\|_X}.$$

4.2. Convergence. Let Π_R, Π_U, Π_Q, and Π_P be the canonical interpolation operators onto the respective finite element spaces, defined for sufficiently regular $(r, u, q, p) \in X$. These operators have the following approximation properties for the finite element families $X_h^{(1)}$ and $X_h^{(2)}$ from (4.1) and (4.2):

$$\|(I - \Pi_R)r\| \lesssim h^{\bar{k}+1}\|r\|_{\bar{k}+1}, \qquad \|\nabla \times (I - \Pi_R)r\| \lesssim h^{k+1}\|\nabla \times r\|_{k+1},$$
$$\|(I - \Pi_U)u\| \lesssim h^{k+1}\|u\|_{k+1}, \qquad \|\nabla \cdot (I - \Pi_U)u\| \lesssim h^{k+1}\|\nabla \cdot u\|_{k+1},$$
$$\|(I - \Pi_Q)q\| \lesssim h^{\bar{k}+1}\|q\|_{\bar{k}+1}, \qquad \|\nabla \cdot (I - \Pi_Q)q\| \lesssim h^{k+1}\|\nabla \cdot q\|_{k+1},$$
$$\|(I - \Pi_P)p\| \lesssim h^{k+1}\|p\|_{k+1}.$$

Here, $\|\cdot\|_k$ denotes the $H^k(\Omega)$-norm and we have $\bar{k} = k$ for $X_h := X_h^{(1)}$ and $\bar{k} = k+1$ for $X_h := X_h^{(2)}$. Let the composite interpolant Π_X be defined for sufficiently regular elements of X such that

$$(4.7) \qquad \Pi_X(r, u, q, p) := (\Pi_R r, \Pi_U u, \Pi_Q q, \Pi_P p).$$

THEOREM 4.3 (Error estimate). *If x, the solution to (3.3), is sufficiently regular, and X_h is chosen as $X_h^{(1)}$ or $X_h^{(2)}$ with polynomial degree $k \geq 0$, then the solution $x_h \in X_h$ to (4.3) converges as*

$$\|x_h - x\|_X \leq C h^{k+1} \Big(h^{\bar{k}-k} \|r\|_{\bar{k}+1} + \|\nabla \times r\|_{k+1} + \|u\|_{k+1} + \|\nabla \cdot u\|_{k+1}$$

(4.8)
$$+ h^{\bar{k}-k} \|q\|_{\bar{k}+1} + \|\nabla \cdot q\|_{k+1} + \|p\|_{k+1} \Big),$$

with $C \geq 0$ possibly depending on the material parameters.

Proof. As shown in the proof of Lemma 4.1, for each $y_h \in X_h$, a $\tilde{y}_h$ exists such that $\langle \mathcal{A} y_h, \tilde{y}_h \rangle \gtrsim \|y_h\|_X^2$ and $\|\tilde{y}_h\|_X \lesssim \|y_h\|_X$. Consider $y_h = x_h - \Pi_X x \in X_h$ and let us use the properties of $\tilde{y}_h$ with the consistency $X_h \subset X$ and continuity of $\mathcal{A}$ from Lemma 3.2 to derive

$$\|x_h - \Pi_X x\|_X^2 \lesssim \langle \mathcal{A}(x_h - \Pi_X x), \tilde{y}_h \rangle = \langle \mathcal{A}(x - \Pi_X x), \tilde{y}_h \rangle$$
$$\lesssim \|(I - \Pi_X) x\|_X \|x_h - \Pi_X x\|_X.$$

A triangle inequality now gives us

$$\|x_h - x\|_X \leq \|x_h - \Pi_X x\|_X + \|(I - \Pi_X) x\|_X \lesssim \|(I - \Pi_X) x\|_X,$$

and the approximation properties of Π_X conclude the proof. $\qquad\square$

5. A multipoint rotation-flux MFE method. We continue by considering the lowest order instance of the finite element family of the second kind, i.e. $X_h^{(2)}$ from (4.2) with $k = 0$. In 3D, this space contains two degrees of freedom per edge for the rotation $r \in \mathbb{N}_1^{(2)}$ and three degrees of freedom per face for the flux $q \in \mathbb{BDM}_1$. By choosing an appropriate quadrature rule for the inner products in R_h and Q_h, we can localize the mass matrix around the vertices. In turn, the variables (r, q) can be eliminated through static condensation and we obtain a multipoint mixed finite element method for the Biot system with $(u, p) \in \mathbb{RT}_0 \times \mathbb{P}_0$ in Subsection 5.1. The stability and convergence of this method are shown in Subsection 5.2.

5.1. Static condensation. Following [14], we consider a specific quadrature rule for functions φ, ϕ on a simplicial mesh:

(5.1)
$$\langle \phi, \varphi \rangle_h := \sum_{\omega \in \Omega_h} \frac{|\omega|}{n+1} \sum_{\boldsymbol{x} \in \mathcal{V}(\omega)} \phi_\omega(\boldsymbol{x}) \cdot \varphi_\omega(\boldsymbol{x})$$

in which ϕ_ω is the restriction of ϕ on an element $\omega \in \Omega_h$ and $\mathcal{V}(\omega)$ is the set of its vertices. The dot product herein reduces to the standard product for scalar ϕ, φ.

We emphasize that $\langle \phi, \varphi \rangle_h$ is non-zero if and only if the basis functions ϕ, φ are non-zero at the same vertex of a mesh element. It has two more advantageous properties, which we highlight in the following lemma.

LEMMA 5.1 ([14, Thm. 4.1]). *The norm $\|\cdot\|_h$ induced by the inner product (5.1) is equivalent to the L^2-norm on R_h and Q_h:*

(5.2) $\|\phi\|_h \eqsim \|\phi\|, \qquad \|\varphi\|_h \eqsim \|\varphi\|, \qquad \forall (\phi, \varphi) \in R_h \times Q_h.$

Moreover, the quadrature rule is exact if the test function is elementwise constant:

(5.3a) $\langle r_h, \mathring{r}_h \rangle_h = \langle r_h, \mathring{r}_h \rangle_\Omega, \qquad \forall r_h \in R_h, \ \mathring{r}_h \in \mathring{R}_h := \mathbb{P}_0^{k_n},$

(5.3b) $\langle q_h, \mathring{q}_h \rangle_h = \langle q_h, \mathring{q}_h \rangle_\Omega, \qquad \forall q_h \in Q_h, \ \mathring{q}_h \in \mathring{Q}_h := \mathbb{P}_0^n.$

We will apply this quadrature rule on the L^2-inner products on the two spaces $R_h \times Q_h$. In particular, we substitute $\langle \cdot, \cdot \rangle_h$ in the definition of A to obtain the discrete operator $A_h : X_h \to X_h'$:

(5.4)
$$\langle A_h x_h, \tilde{x}_h \rangle := \mu^{-1} \langle r_h, \tilde{r}_h \rangle_h + (2\mu + \lambda)\langle \nabla \cdot u_h, \nabla \cdot \tilde{u}_h \rangle_\Omega + \langle K^{-1} q_h, \tilde{q}_h \rangle_h + c_0 \langle p_h, \tilde{p}_h \rangle_\Omega.$$

In turn, we define $\mathcal{A}_h := A_h + B - B^*$, which leads us to the following problem: find $\hat{x}_h \in X_h$ such that

(5.5)
$$\langle \mathcal{A}_h \hat{x}_h, \tilde{x}_h \rangle = \langle f, \tilde{x}_h \rangle, \qquad \forall \tilde{x}_h \in X_h.$$

Next, we aim to eliminate the variables $\hat{r}_h$ and $\hat{q}_h$ to obtain a multipoint mixed finite element method. For that, let us consider the matrix representation of (5.5). Let $\mathsf{M_u}$ and $\mathsf{M_p}$ be the mass matrices on the spaces U_h and P_h, respectively. Moreover, let $\mathsf{M_{r,h}}$ and $\mathsf{M_{q,h}}$ be the matrices corresponding to the quadrature rule, applied to the basis functions of R_h and Q_h. Let $\mathsf{B_r}$, $\mathsf{B_u}$, and $\mathsf{B_q}$ be the representations of the curl on R_h, the divergence on U_h, and the divergence on Q_h, respectively. Finally, to shorten notation, we let $\hat{\mathsf{B}}_\mathsf{r} = \mathsf{M_u B_r}$, $\hat{\mathsf{B}}_\mathsf{u} = \mathsf{M_p B_u}$, and $\hat{\mathsf{B}}_\mathsf{q} = \mathsf{M_p B_q}$ denote the action of these differential operators in their respective range spaces.

Since $\mathsf{M_{r,h}}$ and $\mathsf{M_{q,h}}$ are easily invertible, the variables $\hat{r}_h$ and $\hat{q}_h$ can now be eliminated by taking a Schur complement. We arrive at the algebraic formulation of the *multipoint rotation-flux mixed finite element method (MR-MFEM)*: find $(\hat{u}, \hat{p}) \in U_h \times P_h$ such that

(5.6)
$$\begin{bmatrix} (2\mu + \lambda)\mathsf{B_u^T M_u B_u} + \mu \hat{\mathsf{B}}_\mathsf{r} \mathsf{M_{r,h}^{-1}} \hat{\mathsf{B}}_\mathsf{r}^\mathsf{T} & -\alpha \hat{\mathsf{B}}_\mathsf{u}^\mathsf{T} \\ \alpha \hat{\mathsf{B}}_\mathsf{u} & c_0 \mathsf{M_p} + \delta^2 K \hat{\mathsf{B}}_\mathsf{q} \mathsf{M_{q,h}^{-1}} \hat{\mathsf{B}}_\mathsf{q}^\mathsf{T} \end{bmatrix} \begin{bmatrix} \hat{u} \\ \hat{p} \end{bmatrix} = \begin{bmatrix} \mathsf{f_u} - \mu \hat{\mathsf{B}}_\mathsf{r} \mathsf{M_{r,h}^{-1}} \mathsf{f_r} \\ \mathsf{f_p} - \delta K \hat{\mathsf{B}}_\mathsf{q} \mathsf{M_{q,h}^{-1}} \mathsf{f_q} \end{bmatrix},$$

with $\hat{u}$, $\hat{p}$ the vector representations of $\hat{u}_h$ and $\hat{p}_h$, respectively, and $\mathsf{f} = [\mathsf{f_r}, \mathsf{f_q}, \mathsf{f_u}, \mathsf{f_p}]^T$ representing the right-hand side $f \in X_h'$ in (4.3).

We will refer to (5.5) as the *reducible problem* and the equivalent (5.6) as the *reduced problem*. We remark that (5.6) is a discretization of the following system, in which we recognize the $(1,1)$-block as the weighted vector Laplacian from (2.3):

(5.7)
$$\begin{bmatrix} -\nabla(2\mu + \lambda)\nabla \cdot + \nabla \times \mu \nabla \times & \nabla \alpha \\ \alpha \nabla \cdot & c_0 - \nabla \cdot \delta^2 K \nabla \end{bmatrix} \begin{bmatrix} \hat{u} \\ \hat{p} \end{bmatrix}.$$

REMARK 5.1. *The more general case in which the conductivity K is an element-wise constant, full tensor can be handled by defining a new lumped mass matrix $\mathsf{M_{q,h}^K}$ such that $\mathsf{q^T M_{q,h}^K \tilde{q}} = \langle K^{-1} q, \tilde{q} \rangle_h$ for all $q, \tilde{q} \in Q_h$. However, we restrict our analysis to constant, scalar K and will only consider the more general case in the numerical examples of* Section 7.

5.2. Analysis. We devote this subsection to the theoretical results concerning the MR-MFEM (5.6). After presenting general findings, we present specific results for the two-dimensional case in Subsection 5.2.1.

LEMMA 5.2 (Well-posedness). *The operator $\mathcal{A}_h$ satisfies*

(5.8)
$$\|x_h\|_X \eqsim \sup_{\tilde{x}_h \in X_h} \frac{\langle \mathcal{A}_h x_h, \tilde{x}_h \rangle}{\|\tilde{x}_h\|_X}, \qquad \forall x_h \in X_h.$$

In turn, the reducible problem (5.5) admits a unique and bounded solution $\hat{x}_h \in X_h$.

Proof. The same arguments as in Theorem 4.2 are followed, using the equivalence $\|\cdot\| \approx \|\cdot\|_h$ when necessary. □

As in Lemma 5.1, we let $\mathring{R}_h := \mathbb{P}_0^{k_n}$ with $k_n := \binom{n}{2}$ and $\mathring{Q}_h := \mathbb{P}_0^n$ be the spaces containing elementwise constant (vector) functions. Additionally, let $\mathring{\Pi}_R$ and $\mathring{\Pi}_Q$ be their respective L^2 projections. These have the following approximation properties for sufficiently regular $(r,q) \in R \times Q$:

$$(5.9) \qquad \|(I - \mathring{\Pi}_R)r\| \lesssim h\|r\|_1, \qquad\qquad \|(I - \mathring{\Pi}_Q)q\| \lesssim h\|q\|_1.$$

LEMMA 5.3 (Convergence). *The solution $\hat{x}_h$ to (5.5) converges linearly to x, the solution to (3.3). I.e. a constant C exists, depending on the physical parameters and the regularity of x, such that*

$$(5.10) \qquad\qquad\qquad \|\hat{x}_h - x\|_X \leq Ch.$$

Proof. We follow [14, Thm. 3.2] by first showing that the solutions $\hat{x}_h$ and x_h converge linearly to each other and then using Theorem 4.3 to obtain the result. We start by considering the norm of the difference and use Lemma 5.2 with the fact that $\mathcal{A}x_h = \mathcal{A}_h\hat{x}_h$ to derive:

$$\|\hat{x}_h - x_h\|_X \approx \sup_{\tilde{x}_h \in X_h} \frac{\langle \mathcal{A}_h(\hat{x}_h - x_h), \tilde{x}_h \rangle}{\|\tilde{x}_h\|_X} = \sup_{\tilde{x}_h \in X_h} \frac{\langle (\mathcal{A} - \mathcal{A}_h)x_h, \tilde{x}_h \rangle}{\|\tilde{x}_h\|_X}$$
$$= \sup_{\tilde{x}_h \in X_h} \frac{\langle (A - A_h)x_h, \tilde{x}_h \rangle}{\|\tilde{x}_h\|_X}$$

We continue by bounding the numerator, which consists of the following terms:

$$\langle (A - A_h)x_h, \tilde{x}_h \rangle = \mu^{-1}(\langle r_h, \tilde{r}_h \rangle_\Omega - \langle r_h, \tilde{r}_h \rangle_h) + K^{-1}(\langle q_h, \tilde{q}_h \rangle_\Omega - \langle q_h, \tilde{q}_h \rangle_h)$$

For the first term, we derive the upper bound

$$\mu^{-1}(\langle r_h, \tilde{r}_h \rangle_\Omega - \langle r_h, \tilde{r}_h \rangle_h) = \mu^{-1}(\langle r_h - \mathring{\Pi}_R r, \tilde{r}_h \rangle_\Omega + \langle \mathring{\Pi}_R r - r_h, \tilde{r}_h \rangle_h)$$
$$\leq \mu^{-1}(\|r_h - \mathring{\Pi}_R r\|\|\tilde{r}_h\| + \|\mathring{\Pi}_R r - r_h\|_h\|\tilde{r}_h\|_h)$$
$$\approx \mu^{-1}\|r_h - \mathring{\Pi}_R r\|\|\tilde{r}_h\|$$

The second term is bounded analogously and we obtain

$$\langle (A - A_h)x_h, \tilde{x}_h \rangle \lesssim \mu^{-1}\|r_h - \mathring{\Pi}_R r\|\|\tilde{r}_h\| + K^{-1}\|q_h - \mathring{\Pi}_Q q\|\|\tilde{q}_h\|$$
$$\lesssim (\mu^{-1}\|r_h - \mathring{\Pi}_R r\|^2 + K^{-1}\|q_h - \mathring{\Pi}_Q q\|^2)^{\frac{1}{2}}(\mu^{-1}\|\tilde{r}_h\|^2 + K^{-1}\|\tilde{q}_h\|^2)^{\frac{1}{2}}$$
$$\leq (\mu^{-1}\|r_h - \mathring{\Pi}_R r\|^2 + K^{-1}\|q_h - \mathring{\Pi}_Q q\|^2)^{\frac{1}{2}}\|\tilde{x}_h\|_X$$

Combining with the above, we have thus derived

$$\|\hat{x}_h - x_h\|_X \lesssim (\mu^{-1}\|r_h - \mathring{\Pi}_R r\|^2 + K^{-1}\|q_h - \mathring{\Pi}_Q q\|^2)^{\frac{1}{2}}$$
$$\lesssim \sqrt{\mu^{-1}}(\|r_h - r\| + \|r - \mathring{\Pi}_R r\|) + \sqrt{K^{-1}}(\|q_h - q\| + \|q - \mathring{\Pi}_Q q\|)$$
$$\lesssim \|x_h - x\|_X + \sqrt{\mu^{-1}}\|r - \mathring{\Pi}_R r\| + \sqrt{K^{-1}}\|q - \mathring{\Pi}_Q q\|.$$

Finally, a triangle inequality, property (5.9), and Theorem 4.3 with $k = 0$ give us

$$\|\hat{x}_h - x\|_X \leq \|\hat{x}_h - x_h\|_X + \|x_h - x\|_X \leq Ch. \qquad □$$

13

The introduction of the quadrature rule leaves components of the solution unchanged. We present these invariants formally in the following lemma and subsequent corollaries. The proofs are analogous to [10], but are included here for the sake of completeness.

LEMMA 5.4. *The application of the quadrature rule does not affect the curl of the rotation, i.e.* $\nabla \times \hat{r}_h = \nabla \times r_h$.

Proof. Let $u_r = \nabla \times (\hat{r}_h - r_h)$ and consider the test function $\tilde{x} = (0, u_r, 0, 0)$. Using the fact that $\nabla \cdot u_r = 0$, we derive

$$
\begin{aligned}
0 &= \langle \mathcal{A}_h \hat{x}_h - \mathcal{A} x_h, \tilde{x} \rangle \\
&= \langle \nabla \times (\hat{r}_h - r_h), u_r \rangle_\Omega + (2\mu + \lambda)\langle \nabla \cdot (\hat{u}_h - u_h), \nabla \cdot u_r \rangle_\Omega - \langle \hat{p}_h - p_h, \nabla \cdot \alpha u_r \rangle_\Omega \\
&= \| \nabla \times (\hat{r}_h - r_h) \|^2.
\end{aligned}
$$
□

COROLLARY 5.5. *In the decoupled case of $\alpha = 0$, the volumetric strain is not affected by the quadrature rule. I.e. $\nabla \cdot \hat{u}_h = \nabla \cdot u_h$.*

Proof. Let us consider $\tilde{x} = (0, \hat{u}_h - u_h, 0, 0)$. Using $\nabla \times (\hat{r}_h - r_h) = 0$ from Lemma 5.4 and $\alpha = 0$, we derive:

$$
0 = \langle \mathcal{A}_h \hat{x}_h - \mathcal{A} x_h, \tilde{x} \rangle = (2\mu + \lambda)\| \nabla \cdot (\hat{u}_h - u_h) \|^2.
$$
□

5.2.1. The two-dimensional case. In the special case with $n = 2$, we obtain stronger results concerning the rotation variable, which we present in the following corollary and lemma, respectively.

COROLLARY 5.6. *In 2D, the rotation variable is entirely unaffected by the quadrature rule: $\hat{r}_h = r_h$.*

Proof. In 2D, the curl is given by the rotated gradient $\nabla \times u = (-\partial_2 u, \partial_1 u)$. In turn, Lemma 5.4 implies that $\hat{r}_h - r_h$ is a constant. For $\tilde{x} := (\mu(\hat{r}_h - r_h), 0, 0, 0)$, we derive using $\mathbb{R} \subseteq \mathring{R}_h$ and Lemma 5.1:

$$
\begin{aligned}
0 = \langle \mathcal{A}_h \hat{x}_h - \mathcal{A} x_h, \tilde{x} \rangle &= \langle \hat{r}_h, \hat{r}_h - r_h \rangle_h - \langle r_h, \hat{r}_h - r_h \rangle_\Omega \\
&= \langle \hat{r}_h, \hat{r}_h - r_h \rangle_\Omega - \langle r_h, \hat{r}_h - r_h \rangle_\Omega = \| \hat{r}_h - r_h \|^2.
\end{aligned}
$$
□

LEMMA 5.7 (Improved estimate). *If $n = 2$, then we obtain second order convergence in the rotation variable:*

$$
\tag{5.11} \| \hat{r}_h - r \| = \| r_h - r \| \lesssim h^2 \| r \|_2
$$

Proof. The equality was shown in Corollary 5.6. For the second, we introduce the projection $\mathcal{P}_R : R \to R_h$ obtained by solving the following problem: find $\mathcal{P}_R r \in R_h$ such that

$$
\tag{5.12} \langle \nabla \times \mathcal{P}_R r, \nabla \times \tilde{r}_h \rangle_\Omega = \langle \nabla \times r, \nabla \times \tilde{r}_h \rangle_\Omega, \qquad \forall \tilde{r}_h \in R_h.
$$

In case $\partial_r \Omega = \emptyset$, we set $\langle \mathcal{P}_R, 1 \rangle_\Omega = \langle r, 1 \rangle_\Omega$ to ensure uniqueness. Since $\nabla \times$ is a rotated gradient in 2D, $\mathcal{P}_R r$ is an $\mathbb{L}_1$ approximation of the solution to a Laplace problem, which gives us the approximation property

$$
\tag{5.13} \| (I - \mathcal{P}_R) r \| \lesssim h^2 \| r \|_2.
$$

Let the test function $\tilde{x} := (r_h - \mathcal{P}_R r, \Pi_h(u_h - u), 0, 0)$ with Π_h the L^2 projection onto $\mathrm{Ran}(\nabla\times, R_h) \subseteq Q_h$, as in the proof of Lemma 4.1. We now use $\nabla \cdot \Pi_h = 0$ and the orthogonality property (5.12) to derive

$$
\begin{aligned}
0 = \langle \mathcal{A}(x_h - x), \tilde{x} \rangle &= \mu^{-1} \langle r_h - r, r_h - \mathcal{P}_R r \rangle_\Omega - \langle u_h - u, \nabla \times (r_h - \mathcal{P}_R r) \rangle_\Omega \\
&\quad + \langle \Pi_h(u_h - u), \nabla \times (r_h - r) \rangle_\Omega \\
&= \mu^{-1} \langle r_h - r, r_h - \mathcal{P}_R r \rangle_\Omega - \langle \Pi_h(u_h - u), \nabla \times (I - \mathcal{P}_R) r \rangle_\Omega \\
&= \mu^{-1} \langle r_h - r, r_h - \mathcal{P}_R r \rangle_\Omega \\
&= \mu^{-1} (\| r_h - r \|^2 + \langle r_h - r, (I - \mathcal{P}_R) r \rangle_\Omega)
\end{aligned}
$$

Combining this with (5.13), we arrive at the following bound

$$
\| r_h - r \| = \frac{-\langle r_h - r, (I - \mathcal{P}_R) r \rangle_\Omega}{\| r_h - r \|} \leq \| (I - \mathcal{P}_R) r \| \lesssim h^2 \| r \|_2. \qquad \Box
$$

6. Parameter-robust preconditioning for 4F-MFEM. We follow the preconditioning framework [16], which uses the Riesz representation operator as the canonical preconditioner. In particular, let $\langle \cdot, \cdot \rangle_X$ be the inner product on X that induces the norm $\| \cdot \|_X$ from (3.4). Then we define the preconditioner $\mathcal{P} : X_h' \to X_h$ as the operator that satisfies

$$
(6.1) \qquad \langle \mathcal{P}f, \tilde{x} \rangle_X = \langle f, \tilde{x} \rangle, \qquad\qquad \forall (f, \tilde{x}) \in X_h' \times X_h.
$$

Let $\mathcal{L}(X_h, X_h)$ denote the space of linear maps $X_h \to X_h$ and let $\| \cdot \|_{\mathcal{L}(X_h, X_h)}$ be its norm. From Lemma 3.2, we have $\| \mathcal{P}\mathcal{A} \|_{\mathcal{L}(X_h, X_h)} \lesssim 1$ and, additionally, Lemma 4.1 implies that $\| (\mathcal{P}\mathcal{A})^{-1} \|_{\mathcal{L}(X_h, X_h)}^{-1} \gtrsim 1$. In turn, the condition number of the preconditioned system satisfies

$$
(6.2) \qquad \kappa(\mathcal{P}\mathcal{A}) = \| \mathcal{P}\mathcal{A} \|_{\mathcal{L}(X_h, X_h)} \| (\mathcal{P}\mathcal{A})^{-1} \|_{\mathcal{L}(X_h, X_h)} \lesssim 1.
$$

Since our analysis is based on bounds with constants that are independent of material parameters, this condition number is bounded from above for all admissible parameters. In turn, the operator $\mathcal{P}$ is a parameter-robust preconditioner for 4F-MFEM.

Due to the definition of the norm $\| \cdot \|_X$, the operator $\mathcal{P}$ has a block-diagonal structure with the blocks defined according to their inverses:

$$
\begin{aligned}
\langle \mathcal{P}_r^{-1} r, \tilde{r} \rangle &:= \mu^{-1} (\langle r, \tilde{r} \rangle_\Omega + \langle \nabla \times r, \nabla \times \tilde{r} \rangle_\Omega), \\
\langle \mathcal{P}_u^{-1} u, \tilde{u} \rangle &:= \mu \langle u, \tilde{u} \rangle_\Omega + (2\mu + \lambda) \langle \nabla \cdot u, \nabla \cdot \tilde{u} \rangle_\Omega, \\
\langle \mathcal{P}_q^{-1} q, \tilde{q} \rangle &:= K^{-1} \langle q, \tilde{q} \rangle_\Omega + \frac{\delta^2}{\eta + c_0} \langle \nabla \cdot q, \nabla \cdot \tilde{q} \rangle_\Omega, \quad \langle \mathcal{P}_p^{-1} p, \tilde{p} \rangle := (\eta + c_0) \langle p, \tilde{p} \rangle_\Omega.
\end{aligned}
$$

We emphasize that this preconditioner requires solving independent systems for the variables r, u, q, and p. In order to generate a preconditioner that is scalable for larger systems, these solves can be replaced by spectrally equivalent operators [16]. However, such extensions are beyond the scope of this work.

7. Numerical results. In this section, we present numerical experiments to show the performance of the proposed schemes. We first perform convergence studies in Subsection 7.1 to verify the results from Section 4 and Section 5. Subsequently,

Subsection 7.2 shows the robustness of the preconditioner introduced in Section 6. Finally, Subsection 7.3 presents the approximations for the Mandel problem computed by the proposed four-field and multipoint schemes.

We focus on the lowest order instances of the families of finite elements introduced in Section 4. We refer to the first as the two-field mixed finite element method for elasticity (*2F-MFEM*), respectively the four-field MFEM for poroelasticity (*4F-MFEM*). For the second kind, we apply the quadrature rule from Section 5, and we use the acronym *MR-MFEM* to refer to the resulting multipoint rotation(-flux) mmixed finite element method.

All the numerical results are obtained with the libraries PorePy [13] and Py-GeoN [1]. The scripts of all the test are publicly available at https://github.com/compgeo-mox/rotation_based_biot.

7.1. Convergence study. In this section we evaluate the performance of the method by considering the numerical errors. In particular, we consider problems (2.4) and (2.8) for $n = 2$ and $n = 3$, with the computational domain given by the unit cube $\Omega = (0, 1)^n$. For simplicity, all material parameters are set to 1 and we assume homogeneous essential conditions on $\partial\Omega$.

7.1.1. Linear elasticity. We consider the following exact solutions for $n = 2$ and 3 of Problem (2.4), respectively:

$$(7.1a) \qquad u(x, y) = x^2 y^2 (1 - x)^2 (1 - y)^2 [4, -1]^T,$$
$$(7.1b) \qquad u(x, y, z) = x^2 y^2 z^2 (1 - x)^2 (1 - y)^2 (1 - z)^2 [4, -1, 2]^T,$$

and we set $r = \nabla \times u$. The source term f_u is computed accordingly.

The relative L^2 errors against the analytical solutions are reported in Table 7.1. We notice second order convergence of r for $n = 2$ for both 2F-MFEM and MR-MFEM as shown in Lemma 5.7. In all the other cases, the unknowns converge linearly with respect to the mesh size, as expected by Theorem 4.3 and Lemma 5.3. Moroever, the number of degrees of freedom is significantly smaller for MR-MFEM compared to the 2F-MFEM, and the errors are observed to be larger for the former than for the latter.

In Table 7.2, we compare the solutions of the two methods by computing the relative norms of their differences and associated convergence rates. We observe that the curl of the rotation $\nabla \times r$ and the divergence of the displacement $\nabla \cdot u$ are unaffected by the quadrature rule (5.1), as was shown in Lemma 5.4 and Corollary 5.5, respectively. Moreover, the computated rotation is identical for the two methods if $n = 2$, in agreement with Corollary 5.6.

7.1.2. Poroelasticity. Next, we consider Problem (2.8). Let the exact solutions for the displacement be given by (7.1), while for the flow variables, we consider:

$$q(x, y) = [\sin(2x\pi)\sin(2y\pi), xy(1 - x)(1 - y)]^T, \quad p(x, y) = xy(1 - x)(1 - y),$$

$$q(x, y, z) = \begin{bmatrix} \sin(2x\pi)\sin(2y\pi)\sin(2z\pi) \\ xyz(1-x)(1-y)(1-z) \\ y(1-y)\sin(2x\pi)\sin(2z\pi) \end{bmatrix}, \quad p(x, y, z) = xyz(1-x)(1-y)(1-z).$$

Moreover, we set $r = \nabla \times u$, and the source terms in the second and fourth equations of (2.8a) are computed accordingly. For simplicity we have considered also a vector source term in the third equation of (2.8a), which does not affect the previously introduced theory.

TABLE 7.1
Relative L^2 errors and convergence rates for the solutions r and u, curl of the rotation $\nabla \times r$, and divergence of the displacement $\nabla \cdot u$ against the analytical solutions. Results for the elasticity example in Subsection 7.1.1.

	h	N_{dof}	Err_r	Rate_r	Err_u	Rate_u	$\text{Err}_{\nabla \times r}$	$\text{Rate}_{\nabla \times r}$	$\text{Err}_{\nabla \cdot u}$	$\text{Rate}_{\nabla \cdot u}$
					2F-MFEM					
2 ∥ ≈	6.42e-2	1297	4.72e-3	-	4.47e-2	-	2.19e-2	-	1.85e-1	-
	3.17e-2	4929	1.09e-3	2.07	2.22e-2	1.00	9.92e-3	1.13	9.28e-2	0.98
	1.57e-2	19297	2.47e-4	2.11	1.11e-2	1.00	3.53e-3	1.47	4.66e-2	0.98
	7.83e-3	76465	5.92e-5	2.06	5.52e-3	1.00	1.36e-3	1.37	2.34e-2	0.99
	3.91e-3	304473	1.41e-5	2.07	2.76e-3	1.00	5.00e-4	1.45	1.17e-2	1.00
3 ∥ ≈	2.34e-1	5900	1.14e-1	-	1.02e-1	-	1.95e-1	-	6.12e-1	-
	1.48e-1	22305	6.65e-2	1.18	5.34e-2	1.42	1.41e-1	0.71	3.69e-1	1.10
	1.08e-1	54435	4.26e-2	1.42	3.75e-2	1.13	9.77e-2	1.16	2.73e-1	0.96
	8.58e-2	106001	3.28e-2	1.13	2.88e-2	1.14	8.09e-2	0.81	2.14e-1	1.05
	7.09e-2	185943	2.74e-2	0.96	2.34e-2	1.09	6.56e-2	1.10	1.76e-1	1.03
					MR-MFEM					
2 ∥ ≈	6.42e-2	956	4.72e-3	-	4.46e-2	-	2.19e-2	-	1.85e-1	-
	3.17e-2	3664	1.09e-3	2.07	2.21e-2	0.99	9.92e-3	1.13	9.28e-2	0.98
	1.57e-2	14408	2.47e-4	2.11	1.11e-2	0.99	3.53e-3	1.47	4.66e-2	0.98
	7.83e-3	57220	5.92e-5	2.06	5.52e-3	1.00	1.36e-3	1.37	2.34e-2	0.99
	3.91e-3	228098	1.41e-5	2.07	2.76e-3	1.00	5.00e-4	1.45	1.17e-2	1.00
3 ∥ ≈	2.34e-1	3510	2.67e-1	-	1.11e-1	-	1.95e-1	-	6.12e-1	-
	1.48e-1	13576	1.22e-1	1.71	5.48e-2	1.54	1.41e-1	0.71	3.69e-1	1.10
	1.08e-1	33462	8.16e-2	1.29	3.83e-2	1.15	9.77e-2	1.16	2.73e-1	0.96
	8.58e-2	65554	6.05e-2	1.29	2.92e-2	1.17	8.09e-2	0.81	2.14e-1	1.05
	7.09e-2	115434	4.84e-2	1.17	2.36e-2	1.11	6.56e-2	1.10	1.76e-1	1.03

TABLE 7.2
Relative differences in L^2 between the solutions obtained with 2F-MFEM and MR-MFEM for the rotation r, displacement u, curl of the rotation $\nabla \times r$, and divergence of the displacement $\nabla \cdot u$ of (2.4). Results for the elasticity example in Subsection 7.1.1.

	h	Err_r	Rate_r	Err_u	Rate_u	$\text{Err}_{\nabla \times r}$	$\text{Err}_{\nabla \cdot u}$
				2F-MFEM vs MR-MFEM			
2 ∥ ≈	6.42e-2	1.56e-14	-	1.21e-2	-	7.18e-14	8.97e-15
	3.17e-2	5.02e-14	-	3.08e-3	1.94	3.44e-13	2.40e-14
	1.57e-2	1.21e-13	-	7.71e-4	1.97	1.62e-12	3.97e-14
	7.83e-3	3.33e-13	-	1.93e-4	1.99	7.89e-12	1.07e-13
	3.91e-3	1.22e-12	-	4.82e-5	2.00	3.65e-11	6.30e-13
3 ∥ ≈	2.34e-1	1.54e-1	-	5.61e-2	-	5.52e-14	6.58e-15
	1.48e-1	1.01e-1	0.93	2.21e-2	2.04	3.42e-13	2.26e-14
	1.08e-1	2.16e-2	1.07	1.16e-2	2.06	9.46e-13	4.94e-14
	8.58e-2	5.71e-2	1.01	7.26e-3	2.02	1.39e-12	8.57e-14
	7.09e-2	4.67e-2	1.06	4.91e-3	2.05	3.59e-12	1.89e-13

In Table 7.3 we present the relative L^2 errors against the analytical solutions of the unknowns for both methods in 2D and 3D. We notice that in all cases the errors decay at least with order one, which is expected by Theorem 4.3 and Lemma 5.3. The rotation in 2D is again second order convergent as observed in the previous example and supported by Lemma 5.7. We notice that in 3D, the errors for the MR-MFEM are higher than 4F-MFEM, also higher than in the previous example, probably due to the fact that we are now performing hybridization on two variables. The inital higher order of convergence are due to the high errors obtained on the coarse grids we start with.

Table 7.4 contains the relative L^2 errors for the differentials, i.e. the relevant curl and divergence, of the numerical solutions against their analytical counterparts. Also in this case we obtain at least order one for all variables, in agreement with the theory.

Finally, in Table 7.5 and Table 7.6 we compare the solutions of the two numerical methods by computing the relative norms of their difference. As in the elasticity example, we notice that in 2D the curl of r is unaffected by the quadrature rule (5.1)

TABLE 7.3

Relative L^2 errors and convergence rates for the solutions of (2.8) against the analytical solutions. Results for the poroelasticity example from Subsection 7.1.2.

	h	N_{dof}	Err_r	Rate_r	Err_u	Rate_u	Err_q	Rate_q	Err_p	Rate_p
						4F-MFEM				
	6.42e-2	2869	3.06e-2	-	5.62e-2	-	8.05e-2	-	1.12e-1	-
$n \approx 2$	3.17e-2	10993	7.83e-3	1.93	2.38e-2	1.22	4.01e-2	0.99	5.67e-2	1.22
	1.57e-2	43225	1.95e-3	1.97	1.13e-2	1.06	2.00e-2	0.99	2.84e-2	1.06
	7.83e-3	171661	4.88e-4	2.00	5.55e-3	1.02	9.99e-3	1.00	1.42e-2	1.02
	3.91e-3	684295	1.22e-4	2.00	2.77e-3	1.00	5.00e-3	1.00	7.12e-3	1.00
	2.34e-1	10988	1.32e-1	-	1.41e-1	-	2.87e-2	-	4.48e-1	-
$n \approx 3$	1.48e-1	42227	7.34e-2	1.29	6.50e-2	1.69	1.18e-2	1.95	2.60e-1	1.19
	1.08e-1	103811	4.62e-2	1.48	4.09e-2	1.48	6.22e-3	2.04	1.88e-1	1.04
	8.58e-2	203050	3.49e-2	1.21	3.01e-2	1.32	4.01e-3	1.89	1.46e-1	1.08
	7.09e-2	357203	2.85e-2	1.05	2.42e-2	1.16	2.81e-3	1.87	1.20e-1	1.04
						MR-MFEM				
	6.42e-2	1572	3.06e-2	-	5.55e-2	-	8.05e-2	-	1.15e-1	-
$n \approx 2$	3.17e-2	6064	7.83e-3	1.93	2.37e-2	1.21	4.01e-2	0.99	5.70e-2	0.99
	1.57e-2	23928	1.95e-3	1.97	1.13e-2	1.06	2.00e-2	0.99	2.84e-2	0.99
	7.83e-3	95196	4.88e-4	2.00	5.55e-3	1.02	9.99e-3	1.00	1.42e-2	1.00
	3.91e-3	379822	1.22e-4	2.00	2.76e-3	1.00	5.00e-3	1.00	7.12e-3	1.00
	2.34e-1	5088	2.74e-1	-	1.39e+0	-	1.82e-1	-	1.25e+0	-
$n \approx 3$	1.48e-1	19922	1.26e-1	1.70	5.57e-1	2.01	8.57e-2	1.65	5.39e-1	1.85
	1.08e-1	49376	8.32e-2	1.32	2.93e-1	2.05	5.49e-2	1.43	3.12e-1	1.74
	8.58e-2	97049	6.14e-2	1.31	1.85e-1	1.97	4.17e-2	1.18	2.15e-1	1.61
	7.09e-2	171260	4.90e-2	1.19	1.27e-1	1.98	3.31e-2	1.21	1.61e-1	1.52

TABLE 7.4

Relative L^2 errors for the curl of the rotation $\nabla \times r$, divergence of the displacement and flux $\nabla \cdot u$ and $\nabla \cdot q$, respectively, of (2.8) against the analytical solutions. Results for the poroelasticity example from Subsection 7.1.2.

	h	$\text{Err}_{\nabla \times r}$	$\text{Rate}_{\nabla \times r}$	$\text{Err}_{\nabla \cdot u}$	$\text{Rate}_{\nabla \cdot u}$	$\text{Err}_{\nabla \cdot q}$	$\text{Rate}_{\nabla \cdot q}$
				4F-MFEM			
	6.42e-2	3.38e-2	-	1.86e-1	-	2.25e-1	-
$n \approx 2$	3.17e-2	1.30e-2	1.36	9.29e-2	0.98	1.13e-1	0.97
	1.57e-2	4.35e-3	1.55	4.66e-2	0.98	5.68e-2	0.98
	7.83e-3	1.59e-3	1.45	2.34e-2	0.99	2.84e-2	1.00
	3.91e-3	5.70e-4	1.47	1.17e-2	1.00	1.42e-2	1.00
	2.34e-1	3.22e-1	-	6.70e-1	-	7.31e-1	-
$n \approx 3$	1.48e-1	2.31e-1	0.72	3.79e-1	1.25	4.74e-1	0.95
	1.08e-1	1.61e-1	1.16	2.76e-1	1.02	3.48e-1	0.99
	8.58e-2	1.30e-1	0.91	2.15e-1	1.07	2.77e-1	0.98
	7.09e-2	1.07e-1	1.05	1.77e-1	1.04	2.28e-1	1.01
				MR-MFEM			
	6.42e-2	3.38e-2	-	1.87e-1	-	2.25e-1	-
$n \approx 2$	3.17e-2	1.30e-2	1.36	9.30e-2	0.99	1.13e-1	0.97
	1.57e-2	4.35e-3	1.55	4.66e-2	0.98	5.68e-2	0.98
	7.83e-3	1.59e-3	1.45	2.34e-2	0.99	2.84e-2	1.00
	3.91e-3	5.70e-4	1.47	1.17e-2	1.00	1.42e-2	1.00
	2.34e-1	3.22e-1	-	3.65e+0	-	7.30e-1	-
$n \approx 3$	1.48e-1	2.31e-1	0.72	1.47e+0	1.98	4.74e-1	0.94
	1.08e-1	1.61e-1	1.16	8.01e-1	1.95	3.47e-1	0.99
	8.58e-2	1.30e-1	0.91	5.21e-1	1.85	2.77e-1	0.98
	7.09e-2	1.07e-1	1.05	3.68e-1	1.82	2.28e-1	1.01

in accordance with Lemma 5.4. For the other variables we get at least first order convergence, because both solutions converge linearly to the true solution.

7.2. Parameter-robust preconditioning. In this part, we present the performance of the parameter-robust preconditioner for 4F-MFEM presented in Section 6 on the test case from Subsection 7.1. For this, we first symmetrize the system by negating the second and third rows of $\mathcal{A}$ in (2.8). We then consider the MINRES iterative algorithm with stopping criteria based on relative residual tolerance, which is

TABLE 7.5

Relative differences in L^2 between the solutions obtained with the 4F-MFEM and MR-MFEM scheme for the rotation r, displacement u, flux q, and pressure p. Results for the poroelasticity example in Subsection 7.1.2.

	h	Err_r	Rate_r	Err_u	Rate_u	Err_q	Rate_q	Err_p	Rate_p
	6.42e-2	1.13e-13	-	1.35e-2	-	7.66e-4	-	2.23e-2	-
$n=2$	3.17e-2	3.17e-13	-	3.37e-3	1.97	2.74e-4	1.46	5.60e-3	1.96
	1.57e-2	9.82e-13	-	8.39e-4	1.98	8.20e-5	1.71	1.40e-3	1.97
	7.83e-3	1.38e-12	-	2.10e-4	1.99	3.13e-5	1.38	3.52e-4	1.99
	3.91e-3	7.31e-12	-	5.24e-5	2.00	1.08e-5	1.54	8.80e-5	2.00
	2.34e-1	1.58e-1	-	7.88e-1	-	3.72e-1	-	7.47e-1	-
$n=3$	1.48e-1	1.02e-1	0.97	4.80e-1	1.08	1.40e-1	2.14	4.22e-1	1.25
	1.08e-1	7.25e-2	1.08	2.71e-1	1.82	7.83e-2	1.86	2.35e-1	1.87
	8.58e-2	5.72e-2	1.03	1.75e-1	1.90	5.43e-2	1.58	1.51e-1	1.90
	7.09e-2	4.67e-2	1.06	1.20e-1	1.96	4.05e-2	1.54	1.03e-1	1.99

TABLE 7.6

Relative differences in L^2 between the curl of the rotation $\nabla \times r$, divergence of the displacement $\nabla \cdot u$, and divergence of the flux $\nabla \cdot q$ of the solutions obtained with the 4F-MFEM and MR-MFEM. Results for the poroelasticity example in Subsection 7.1.2.

	h	$\mathrm{Err}_{\nabla \times r}$	$\mathrm{Err}_{\nabla \cdot u}$	$\mathrm{Rate}_{\nabla \cdot u}$	$\mathrm{Err}_{\nabla \cdot q}$	$\mathrm{Rate}_{\nabla \cdot q}$
	6.42e-2	3.35e-13	1.63e-2	-	3.58e-4	-
$n=2$	3.17e-2	1.75e-12	4.11e-3	1.95	9.00e-5	1.96
	1.57e-2	1.03e-11	1.03e-3	1.97	2.26e-5	1.97
	7.83e-3	3.73e-11	2.59e-4	1.99	5.65e-6	1.99
	3.91e-3	1.90e-10	6.47e-5	2.00	1.41e-6	2.00
	2.34e-1	6.35e-13	9.56e-1	-	4.55e-3	-
$n=3$	1.48e-1	9.37e-12	8.49e-1	0.26	1.82e-3	2.01
	1.08e-1	1.03e-11	6.22e-1	0.99	9.57e-4	2.05
	8.58e-2	3.33e-11	4.40e-1	1.50	6.05e-4	1.98
	7.09e-2	5.48e-11	3.12e-1	1.80	4.12e-4	2.01

set to 10^{-5}. In Figure 7.1 we present the number of iterations obtained for $n = 2$ and 3 for a wide range of the material parameters. We see that the number of iterations is stable for most of the parameter values. We notice a slight dependency in a few cases, but the number of iterations remains moderate.

Finally, we have applied the same strategy for the elasticity problem (2.4), which can be seen as the limit case of $\alpha = 0$. By varying its parameters and mesh size, we obtain a stable number of iterations between 2 and 5 (not reported in a figure), confirming the robustness of the preconditioner.

7.3. Mandel's problem. In this section we consider Mandel's test case [3], which admits an exact solution in 2D and exhibits interesting time-dependent effects. Let us consider a two-dimensional, poroelastic domain between two rigid plates on the upper and bottom boundaries of the domains, that are free to slide. A force of $2F$ is applied on the plates causing a uniform displacement $\nu \cdot u$ that is independent of x. The domain is displayed in the left of Figure 7.2. Due to the symmetries of the problem, we consider a quarter of the domain. Classically, the following boundary conditions are applied:

$$\nu \cdot u = 0, \qquad \nu \times (\sigma\nu) = 0, \quad \nu \cdot q = 0, \quad \text{on } \Gamma_1 \cup \Gamma_2,$$
$$\sigma\nu = 0, \qquad p = 0, \quad \text{on } \Gamma_3,$$
$$\nu \cdot u = \text{const}, \quad \frac{1}{a} \int_{\Gamma_4} \nu \cdot (\sigma\nu) = -2F, \quad \nu \times (\sigma\nu) = 0, \quad \nu \cdot q = 0 \quad \text{on } \Gamma_4.$$

We adapt these conditions to our formulation of the problem by setting $\partial_u \Omega = \partial\Omega$, $\partial_p \Omega = \Gamma_3$, and $\partial_q \Omega = \partial\Omega \backslash \Gamma_3$. First, on Γ_1 and Γ_2, we set $\nu \cdot u = 0$ and, together with
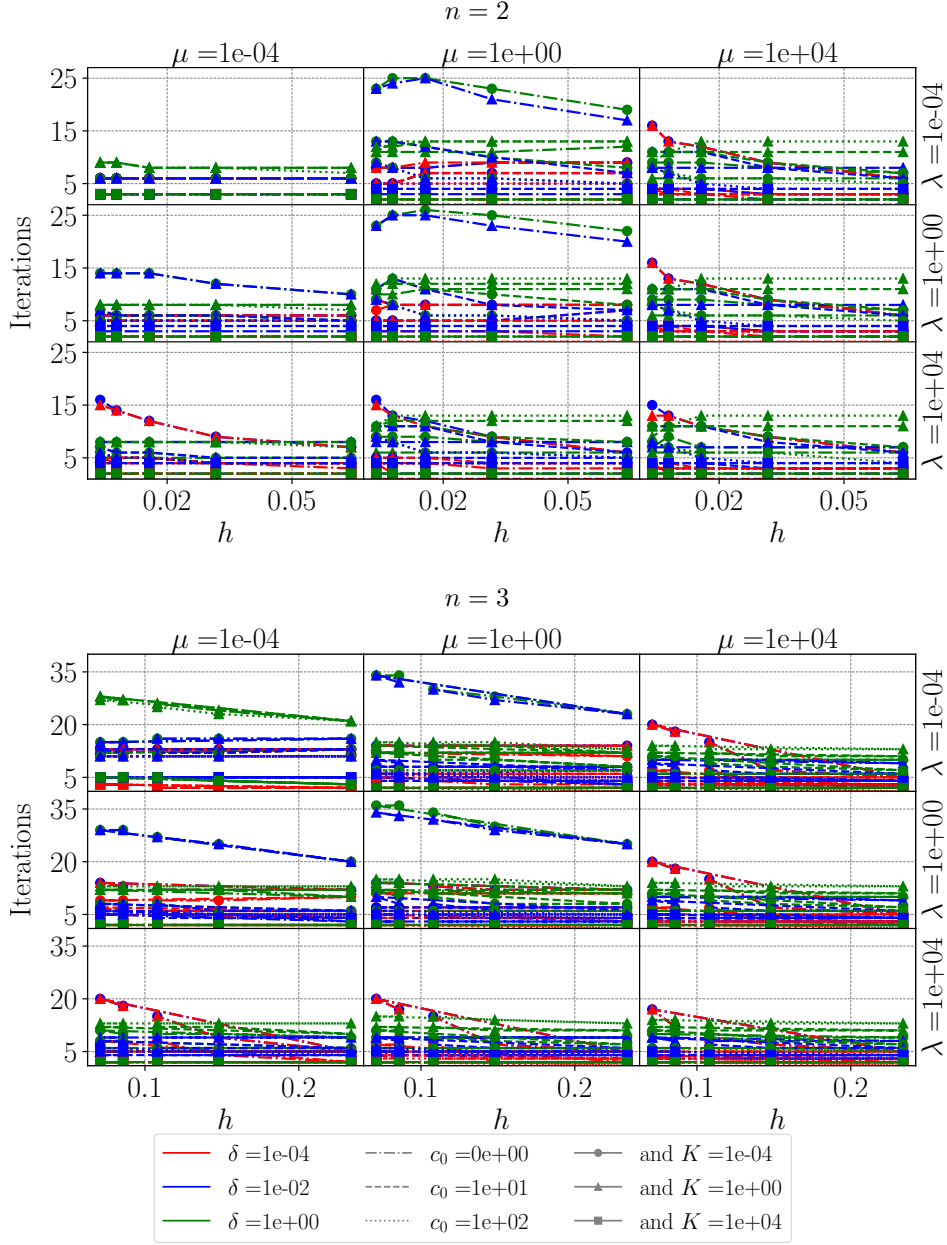
FIG. 7.1. *The number of MINRES iterations remains stable for a wide range of parameter values when applying the proposed preconditioner.*

$\nu \times (\sigma \nu) = 0$, we obtain $r = 0$, which is set as an essential condition. On the other hand, on Γ_3 and Γ_4, we set $\nu \cdot u$ to be equal to the analytical solution and $r = 0$. The exact solution for pressure, displacement and stress can be expressed as a series as in [18].

The values of the geometric and material parameters are reported in the table in the right of Figure 7.2. Figure 7.3 illustrates the numerical results obtained with both

FIG. 7.2. *(left) The domain for the Mandel's problem and (right) the material and geometric parameters.*
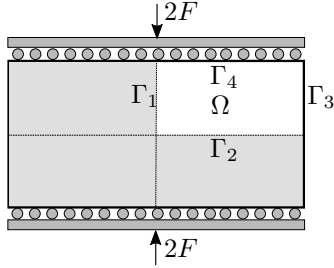
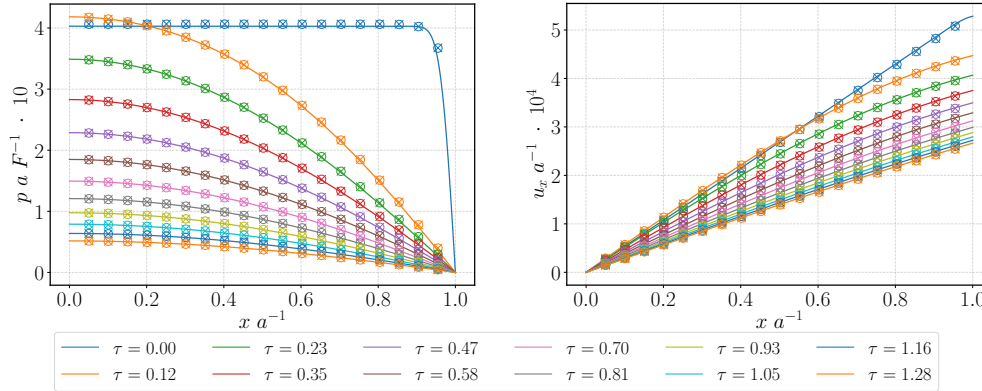|			
$a =$	100	$\mu =$	2.475e9
$b =$	10	$\lambda =$	1.65e9
$T =$	5e4	$\alpha =$	1
$\Delta t =$	1e1	$c_0 =$	6.0606e-11
$F =$	6e8	$K =$	9.869e-11

FIG. 7.3. *The scaled pressure (left) and the scaled displacement (right) along the x axis, for different times. The continuous lines represent the analytical solution at different times τ. The $\circ$ and $\times$ markers are the solutions computed by 4F-MFEM and MR-MFEM, respectively.*

4F-MFEM and MF-MFEM, with the analytical solutions. Excellent matching is observed for both schemes. Moreover, we obtain zero rotation, numerically, everywhere in the domain, which corresponds exactly to the zero rotation in the true solution.

8. Concluding remarks. We have proposed mixed finite element methods for rotation-based poroelasticity in which the rotation variable is approximated in $H(\nabla\times,\Omega)$. Through a hybridization technique, the rotation and flux variables can be locally eliminated, leading to a numerical scheme that uses $\mathbb{RT}_0 \times \mathbb{P}_0$ for the solid displacement and fluid pressure. A priori analysis shows that the proposed methods are stable and convergent. By using weighted norms, we moreover derive robust preconditioners.

We remark on the limitations of our approach. First, we note that the formulation (2.3) of the elasticity equations as a weighted vector Laplacian is based on a spatially constant Lamé parameter μ. However, the techniques from [6] may be applicable for the more general case of varying μ. Second, the natural boundary conditions for this formulation do not immediately accommodate the typical no-stress boundary condition. In our implementation of Mandel's problem, we therefore augmented the boundary conditions. Third, we note that nearly incompressible materials are not naturally handled by this formulation since large values of λ lead to undesirable scaling in the matrix. To capture the incompressible limit of $\lambda \to \infty$, it may be desirable to introduce a solid pressure variable similar to [15]. We aim to overcome

these limitations in future work.

Finally, the numerical results presented show optimal convergence rates and, when the preconditioner is applied, a stable number of iterations for a wide range of data values, all in accordance with the developed theory.

REFERENCES

[1] *PyGeoN: a Python package for Geo-Numerics*, https://doi.org/10.5281/zenodo.7437428.

[2] I. AAVATSMARK, *An introduction to multipoint flux approximations for quadrilateral grids*, Computational Geosciences, 6 (2002), pp. 405–432.

[3] Y. ABOUSLEIMAN, A. H.-D. CHENG, L. CUI, E. DETOURNAY, AND J.-C. ROEGIERS, *Mandel's problem revisited*, Gèotechnique, 46 (1996), pp. 187–195, https://doi.org/10.1680/geot.1996.46.2.187.

[4] I. AMBARTSUMYAN, E. KHATTATOV, J. M. NORDBOTTEN, AND I. YOTOV, *A multipoint stress mixed finite element method for elasticity on simplicial grids*, SIAM Journal on Numerical Analysis, 58 (2020), pp. 630–656.

[5] I. AMBARTSUMYAN, E. KHATTATOV, AND I. YOTOV, *A coupled multipoint stress–multipoint flux mixed finite element method for the biot system of poroelasticity*, Computer Methods in Applied Mechanics and Engineering, 372 (2020), p. 113407.

[6] V. ANAYA, R. CARABALLO, B. GÓMEZ-VARGAS, D. MORA, AND R. RUIZ-BAIER, *Velocity-vorticity-pressure formulation for the oseen problem with variable viscosity*, Calcolo, 58 (2021), pp. 1–25.

[7] V. ANAYA, Z. DE WIJN, B. GÓMEZ-VARGAS, D. MORA, AND R. RUIZ-BAIER, *Rotation-based mixed formulations for an elasticity-poroelasticity interface problem*, SIAM Journal on Scientific Computing, 42 (2020), pp. B225–B249.

[8] V. ANAYA, Z. DE WIJN, D. MORA, AND R. RUIZ-BAIER, *Mixed displacement–rotation–pressure formulations for linear elasticity*, Computer Methods in Applied Mechanics and Engineering, 344 (2019), pp. 71–94.

[9] D. N. ARNOLD, R. S. FALK, AND J. GOPALAKRISHNAN, *Mixed finite element approximation of the vector laplacian with dirichlet boundary conditions*, Mathematical Models and Methods in Applied Sciences, 22 (2012), p. 1250024.

[10] W. M. BOON AND A. FUMAGALLI, *A multipoint vorticity mixed finite element method for incompressible Stokes flow*, Applied Mathematics Letters, (2022), p. 108498.

[11] F. BREZZI, J. DOUGLAS, AND L. D. MARINI, *Two families of mixed finite elements for second order elliptic problems*, Numerische Mathematik, 47 (1985), pp. 217–235.

[12] S. CAUCAO, T. LI, AND I. YOTOV, *A multipoint stress-flux mixed finite element method for the Stokes-Biot model*, Numerische Mathematik, 152 (2022), pp. 411–473.

[13] E. KEILEGAVLEN, R. BERGE, A. FUMAGALLI, M. STARNONI, I. STEFANSSON, J. VARELA, AND I. BERRE, *Porepy: An open-source software for simulation of multiphysics processes in fractured porous media*, Computational Geosciences, 25 (2021), pp. 243–265.

[14] J. LEE AND R. WINTHER, *Local coderivatives and approximation of hodge laplace problems*, Mathematics of Computation, 87 (2018), pp. 2709–2735.

[15] J. J. LEE, E. PIERSANTI, K.-A. MARDAL, AND M. E. ROGNES, *A mixed finite element method for nearly incompressible multiple-network poroelasticity*, SIAM journal on scientific computing, 41 (2019), pp. A722–A747.

[16] K.-A. MARDAL AND R. WINTHER, *Preconditioning discretizations of systems of partial differential equations*, Numerical Linear Algebra with Applications, 18 (2011), pp. 1–40.

[17] J.-C. NÉDÉLEC, *Mixed finite elements in* $\mathbb{R}^3$, Numerische Mathematik, 35 (1980), pp. 315–341.

[18] P. PHILLIPS AND M. WHEELER, *A coupling of mixed and continuous Galerkin finite element methods for poroelasticity I: the continuous in time case*, Comput Geosci, 11 (2007), pp. 131–144.

[19] C. RODRIGO, X. HU, P. OHM, J. H. ADLER, F. J. GASPAR, AND L. ZIKATANOV, *New stabilized discretizations for poroelasticity and the Stokes' equations*, Computer Methods in Applied Mechanics and Engineering, 341 (2018), pp. 467–484.

[20] M. F. WHEELER AND I. YOTOV, *A multipoint flux mixed finite element method*, SIAM Journal on Numerical Analysis, 44 (2006), pp. 2082–2106.

MOX Technical Reports, last issues

Dipartimento di Matematica

Politecnico di Milano, Via Bonardi 9 - 20133 Milano (Italy)

01/2023   Zingaro, A.; Bucelli, M.; Piersanti, R.; Regazzoni, F.; Dede', L.; Quarteroni, A.

An electromechanics-driven fluid dynamics model for the simulation of the whole human heart

82/2022   Ciaramella, G.; Gander, M.; Van Criekingen, S.; Vanzan, T.

A PETSc Parallel Implementation of Substructured One- and Two-level Schwarz Methods

81/2022   Bonizzoni, F.; Hauck, M.; Peterseim, D.

A reduced basis super-localized orthogonal decomposition for reaction-convection-diffusion problems

84/2022   Ciaramella, G.; Gambarini, M.; Miglio, E.

A preconditioner for free-surface hydrodynamics BEM

85/2022   Lurani Cernuschi , A.; Masci, C.; Corso, F.; Muccini, C.; Ceccarelli, D.; San Raffaele Hospital
Galli, L.; Ieva, F.; Paganoni, A.M.; Castagna, A.

A neural network approach to survival analysis for modelling time to cardiovascular diseases in HIV patients with longitudinal observations

83/2022   Ciaramella, G.; Gander, M.; Mazzieri, I.

Unmapped tent pitching schemes by waveform relaxation

80/2022   Balduzzi, G.; Bonizzoni, F.; Tamellini, L.

Uncertainty quantification in timber-like beams using sparse grids: theory and examples with off-the-shelf software utilization

78/2022   Bucelli, M.; Gabriel, M. G.; Gigante, G.; Quarteroni, A.; Vergara, C.

A stable loosely-coupled scheme for cardiac electro-fluid-structure interaction

79/2022   Antonietti, P. F.; Farenga, N.; Manuzzi, E.; Martinelli, G.; Saverio, L.

Agglomeration of Polygonal Grids using Graph Neural Networks with applications to Multigrid solvers

77/2022   Ziarelli, G.; Dede', L.; Parolini, N.; Verani, M.; Quarteroni, A.

Optimized numerical solutions of SIRDVW multiage model controlling SARS-CoV-2 vaccine roll out: an application to the Italian scenario.